Modelling earthquake induced hazards alongside probabilistic risk assessment: A pilot study of Napier

K.E. Jones, J. Moratalla., S.R. Uma, D. Burbidge, J. Roger, A.G. Griffin, C. Mueller, F. Scheele, E. Bretherton & Y. Mahmood

GNS Science Te Pū Ao, Lower Hutt, New Zealand.

ABSTRACT

Earthquakes are a known trigger of cascading hazards, with the sequence of secondary events often resulting in a significantly higher impact. In Aotearoa, once such source of potentially devasting events is the Hikurangi Subduction Zone (HSZ). With an estimated maximum credible earthquake of ~Mw 9.1, a HSZ earthquake event is likely to induce a large number of secondary hazards and cause substantial disruption to the nearby built environments along the east coast of the North Island. Disaster risk reduction and resilience planning for such events requires an understanding of the secondary processes and their extent, with this information presented in in useful and well-recognised metrics. For our Napier case study, we developed a cascading hazards probabilistic risk assessment approach capable of quantifying the impact caused by an HSZ earthquake to the built environment. The primary and secondary earthquake impacts included in this analysis were ground shaking, tsunamis, landslides and liquefaction. Uncertainties for each hazard were concatenated in a Monte Carlo based framework that links to damage functions to estimate impact to buildings. Overall results show that damage is driven by earthquake shaking and liquefaction, followed by tsunami, lateral spreading and landslides, depending on the annual exceedance probabilities (AEP). Disaggregation of losses to the different types of cascading hazards can inform decision makers on how to optimise their resilience investment planning to minimise impact.

1 INTRODUCTION

The Hikurangi Subduction Zone (HSZ) off the east coast of the North Island of New Zealand, where the western Pacific Plate subducts under the Australian Plate, is potentially the earthquake source with largest possible magnitude in New Zealand. Megathrust faults along the interface of subducting plates are responsible for the largest and most powerful earthquakes in the world, such as the 2004 Mw 9.3 Sumatra, 2010 Mw 8.8 Chile, and 2011 Mw 9.1 Tohoku (Japan) earthquakes. An earthquake on the Hikurangi margin could trigger a cascading sequence of hazards that would have a significant impact on New Zealand communities, assets, and the national economy, e.g. widespread ground shaking, landslides, tsunami, fires, onshore ground subsidence, liquefaction, and further large earthquakes via a prolonged sequence of aftershocks. To better prepare for, and mitigate, the effects of a large earthquake on the HSZ, the combined perils that could be caused by the earthquake should be considered with a "multi-hazard" approach.

1.1 Objectives of the pilot study

The aim of the work presented here is to create a probabilistic framework for quantitatively estimating the impacts in terms of monetary loss ratios from HSZ earthquakes, including the cascading sequence of possible hazards trigged by the initial earthquake. The losses from perils include ground shaking, landsliding, liquefaction and tsunamis caused by offshore crustal deformation. The combined losses from these cascading effects are estimated on a portfolio of residential and commercial buildings in the region. The uncertainty in quantifying these hazards, and the damage they cause, are concatenated using a Monte Carlo Simulation approach that provides a quantitative estimate of the combined losses from shaking and its cascading effects. The framework was tested using a case study for Napier City and applied to buildings extracted from the national building inventory compiled by Scheele et al. (2023). Potential users of these risk metrics include insurers and reinsurers, asset owners, emergency managers, and government agencies. These risk outputs can also be utilized for planning, prioritizing mitigation efforts, enhancing preparedness and resilience against cascading earthquake hazards, and budgeting for the recovery from such events.

1.2 Napier City

Napier City, in the Hawke's Bay region, was the case study for developing and testing the probabilistic framework. Sitting above the Hikurangi subduction zone interface (Williams et al., 2013), Napier is located on the east coast of the North Island of New Zealand and is less than 200 km away from the subduction trench (Fig. 1a). This exposes Napier's inhabitants to significant amounts of earthquake risk, from both the Hikurangi subduction interface itself and upper-plate faults extending up from it (Delano et al. 2023). In the last century, Napier has experienced the deadliest earthquake in New Zealand's history, the 1931 Mw 7.4 - 7.6 Hawke's Bay earthquake (also known as the Napier Earthquake). The official death toll for the Hawke's Bay earthquake was 256 and >400 people sustained serious injuries. There was also noticeable uplift, liquefaction, lateral spreading and landsliding along with major damage to buildings and infrastructure across the built-up areas of Napier and Hastings (McGregor, 1998).

2 METHODOLOGY

2.1 A Monte-Carlo based approach for cascading hazards impact estimation

In this study, a Monte Carlo Simulation based approach (MCS) was proposed to estimate the impact of an earthquake event and cascading hazards to the built environment. MSC allows for generating damage scenarios that are derived through the concatenation of random sampling of the hazard intensities and the fragility functions for every earthquake event considered. The calculation of a damage scenario for an event in the stochastic catalogue or for a given scenario analysis consists of several main steps:

1. Synthetic earthquake catalogue – we generated a stochastic catalogue of earthquakes of 100,000 years using and Event-based Probabilistic Seismic Hazard Analysis using OpenQuake (GEM, 2019), and the magnitude-frequency distribution parameters proposed for the HSZ in the New Zealand National Seismic Hazard Model (Gerstenberger, 2022).

2. Ground motions - for a given earthquake event in the stochastic catalogue, ground motion prediction equations (GMPEs) were used to estimate the ground motion intensity parameters (e.g., PGA, PGV).
3. Tsunami inundation models - we use a pre-calculated a database of scenario inundation scenarios for Napier for a range of HSZ earthquake rupture geometries, magnitudes, locations, and slip distributions. The inundation depths obtained for simulation are mapped to the building locations.
4. Liquefaction severity modelling - the earthquake conditions are combined with the volumetric strain of the soil (obtained through geotechnical analyses) to estimate a Liquefaction Severity Number value (LSN, Tonkin and Taylor, 2013). For a given PGA, LSN follows a normal distribution in a defined liquefaction susceptibility zone. At each site, LSN is randomly sampled from this normal distribution and mapped to the building locations.
5. Lateral spreading modelling - we use the lateral displacement index (LDI) parameter (Zhang et al, 2004) to generate estimations of the expected lateral displacement due to liquefaction at each building location. This requires topographical analysis of the site, including ground slope, direction, distance to a free face and height of the free face, and the geotechnical conditions of the saturated layers of soil.
6. Earthquake-induced landslides modelling - earthquake induced landslide (EIL) probabilities are calculated using the earthquake-induced landslide forecast tool (Massey et al 2021, 2023). Then empirical relationships of landslide size and runout are used to estimate the debris inundation zone and for each earthquake, the EIL probabilities are mapped to buildings within the debris inundation zone.
7. Damage modelling - for each building in the portfolio the appropriate fragility function for each peril is selected. The relevant hazard intensity metric was then used to determine the likelihood of the building becoming damaged (represented by its Damage State, DS). For a given MSC run, these fragility functions are used to determine the damage state of the building. The building is assumed to reach a final damage state which is the combination of damage states from each cascading peril in the run. Two combinations of DS were explored in this study, i) selecting the maximum damage state obtained across all perils site to calculate the loss from an assumed damage ratio, and ii) aggregating losses from minor to moderate damage states and taking the maximum for severe to complete damage states.
8. Loss Ratios (LR) - are assigned to each DS, for each building in the portfolio. Uncertainties in the assigned LRs are quantified using a probability density function normally distributed around the mean LR for each DS.

Each of the above steps were repeated 100 times for each event in the synthetic catalogue, to capture the intra event loss variability (i.e., variability due to uncertainties from the different hazards, vulnerabilities and LR assignations). Losses from all the events were aggregated and the risk metrics (e.g., annual exceedance probability curves, or average annual MDRs) were calculated. Post-earthquake hazards were out of scope.

2.2 Hazard modelling

Due to the short format of the conference paper, we focus on explaining the approach to modelling the EIL hazard only. More detailed information about the hazard modelling can be found in Moratalla et al., 2024.

2.3 Earthquake induced landslides

The terrestrial landslide hazard was estimated using version V2.1 of the EIL susceptibility model (Massey et al., 2021; 2023). This statistical model is based on the logistic regression machine learning approach, that predicts the spatial distribution of earthquake induced landslide probability at the regional scale for different levels of earthquake ground shaking (PGA). We then followed the hazard and risk methodology described by

Brideau et al. (2020), and the empirical landslide relationships complied by Brideau et al. (2021) to define the landslide sources and model landslide runout, which are not an output of the EIL forecast tool. This approach consisted of several steps:

1. EIL forecast tool – we ran the EIL tool 10 times using uniform PGA values of 0.2g, 0.3g, 0.4g, 0.5g, 0.75g, 1g, 1.5g, 2g, 2.5g and 3g. This span of PGA values represents the range of possible ground shaking up to the maximum earthquake modelled in the stochastic catalogue (M_w9.1 HSZ earthquake).
2. Define slope units – we used slope unit polygons to separate out individual hillslope faces which can generate individual landslides (Fig. 1b-c). We then identified source regions within these slope units.
3. Define source regions - to represent the potential landslide locations, source regions were determined using empirical relationships slope, local slope relief (LSR) and landslide occurrence for each slope unit. For each source region we determined the maximum credible volume class (MCVS) using Table 1.
4. Calculate landslide probability - the probability of each volume class occurring was estimated using empirical relationships These empirical relationships were determined from the co-seismic landslide inventory for the 2016 Mw 7.8 Kaikōura earthquake and contains <30,000 landslides (Jones et al. 2024). For each landslide class (up to the MSCV), within each source region, we summed the EIL tool output probabilities for each PGA input value.

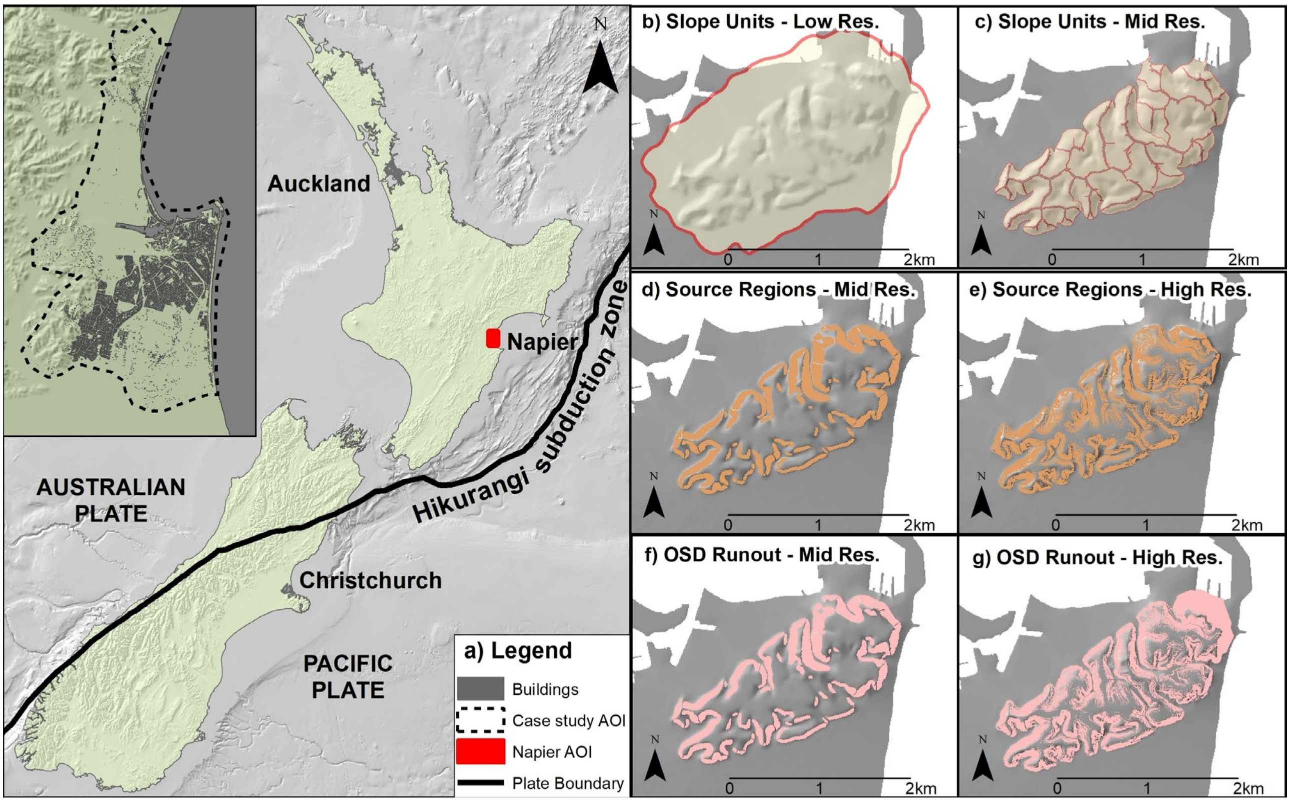

Figure 1a: Location of Napier City in relation to the HSZ. (insert map) Location of the 115 km² case study AOI and buildings used to estimate the economic impact of an earthquake. b-c) Comparison of the different methods used to determine the slope units (low resolution = r.slopeunits; mid resolution = 8 m DEM). d-g) Comparison of the DEM used to determine the source regions and landslide runout (mid resolution = 8 m DEM; high resolution = 3 m DEM).

5. Model runout distance – for each volume class, within each source region, we used a given Fahrböschung angle estimated from a compilation of global data (Brideau et al. 2021; Table 1). The

Fahrböschung angle is the angle between the landslide source and the landslide deposit, using the ratio of elevation difference and horizontal distance between the crest of the landslide source and distal toe of the deposit (Fig. 2a). The Fahrböschung angle was projected as the maximum distance for runout from each cell within the source region and used to create landslide debris polygons for each volume class.

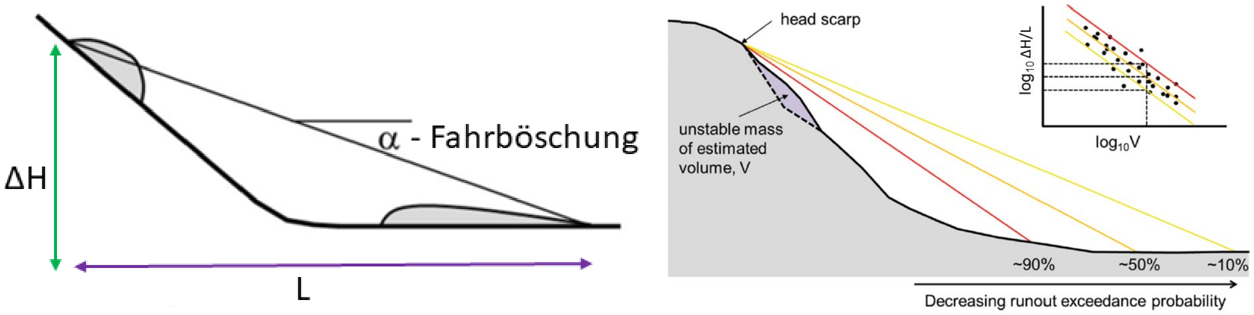

Figure 2a: Schematic representation of the fall height (ΔH) and runout distance (L) parameters for a landslide. b) Schematic representation of runout exceedance probability based on empirical relationships. (Figure modified from McDougall 2017).

Debris inundation relationships have been established for these three types of landslides initiated under 'dry' or 'wet' conditions; these being: (1) open slope dry rock and debris avalanches (OSD); (2) open slope wet debris avalanches (OSW), and (3) channelized wet debris flows (CHW). OSD debris avalanches are triggered by earthquakes, while OSW debris avalanches and CHW debris flows are triggered by rainfall. Thus, only OSD rock avalanche relationships were used in this study. The landslide debris inundation extents were estimated based on the 50% runout Probability of Exceedance (POE) for given volume class (Fig. 2b).

Table 1: Landslide volume classes, their properties used to assign source regions to each class and probability.

Class	Volume (m3)	Max Area (m2)	LSR (m)	Fahrböschung (OSD)	Obstacle	Probability
2	32	200	25	41.62	0	0.5969
3	316	1600	29	39.46	0.5	0.4802
4	3,162	12,000	39	37.33	1	0.1100
5	31,623	89,000	51	27.57	1	0.0107
6	316,228	675,000	66	20.88	1	0.0010
7	3,162,278	999,999,999	71	43.79	1	0.0003

2.3.1 Refining the slope units

The above workflow was first applied using geomorphological slope units derived using the r.slopeunits software (Alvioli et al. 2016) for the whole of New Zealand. Then to refine the slope units, we developed a new approach using the 8m Geographx DEM (https://data.linz.govt.nz/layer/51768-nz-8m-digital-elevation-model-2012/). The 8m Geographx DEM was chosen over the LiDAR derived DEM to reduce the influence of micro topography within hillslope facets. We removed slopes <10 degrees (flat terrain) and the remaining slopes were separated into units using ridgelines and prominent spurs running down between the hillslope facets. In a GIS environment, we used flow direction and flow accumulation hydrology tools to identify divergent cells (which represented ridgelines and spurs). Manual editing of the individual slope units was required to divide the larger hillslope facets representing catchments with steep narrow channels.

2.3.2 Testing the influence of DEM resolution on defining landslide source regions and landslide debris inundation extents

To understand how DEM resolution influenced the landslide modelling, we used two difference resolution DEMs; i) 8m Geographx DEM and ii) a 3m lidar DEM covering the Napier study area (https://data.linz.govt.nz/layer/112889-hawkes-bay-lidar-1m-dem-2020-2021/), to create the slope regions and to project the Fahrböschung angle. The higher resolution DEM is more likely to capture the influence of micro topographic features at the hillslope scale which influences the MCVC and runout distance.

3 RESUTS AND DICUSSION

3.1 Influence of DEM resolution on landslide hazard and risk

Within the 115 km^2 Napier case study AOI, there were 131 slope units derived using the r.slopeunits software (Alvioli et al. 2016), which ranged in size from 50,000 m^2 to 5,000,000 m^2. These slope units were too coarse to be useful for this case study within the Napier area as they span across ridgelines or multiple hillslope facets (Fig. 1b). In contrast there were 407 slope units derived from the 8m Geographx DEM using the slope threshold and divergent flow approach. These slope units, which ranged in size from 500 m^2 to 30,000 m^2, were a better representation of the hillslope facets (Fig. 1c), so were used in the MCS approach. Source regions were calculated at two resolutions, using the 8m Geographx DEM (mid resolution) and a 3 m resampled Lidar DEM (high resolution).

The 8 m source regions covered a total area of 7.20 km^2 and went up to volume class 6, while the 3m source regions covered a total area of 10.93 km^2 and went up to volume class 7 (Table 2). Landslide runout (OSD) was also calculated at two resolutions, using the 8m Geographx DEM (with the 8 m source regions) and the 3 m DEM (with the 3 m source regions). The total area of debris inundation at mid resolution (8 m) was 10.42 km^2 and impacted 870 buildings. The total area of debris inundation at high resolution (3 m) was 11.14 km^2 and impacted 1005 buildings (Table 2). Due to the more realistic modelling of potential landslide sources and runout, we used the source regions and runout model outputs at 3 m for the MCS approach.

Table 2: Differences in the coverage of slope units, source regions and debris inundation due to DEM resolution across the 115 km2 Napier case study AOI. Note sources area only occurred on slopes

Resolution	*DEM input*	*Slope Unit (total coverage)*	*Source Region (total coverage)*	*Max. credible Volume Class*	*OSD Runout (total coverage)*	*Debris inundation (no. buildings impacted)*
High	3m DEM	-	10.93 km^2	7	11.14 km^2	1005
Med	8m DEM	16.48 km^2	7.20 km^2	6	10.42 km^2	870
Low	8m DEM	32.94 km^2	-	-	-	-

3.2 Multi-peril cascading hazard and risk model for Napier

By combining the hazard values with the exposure and fragility curves, we could calculate the losses caused by the different hazards for each event in the stochastic earthquake catalogue. Resulting mean damage ratios can be presented as exceedance probability curves (EP curves) for a given time interval (e.g., 1 year), or return period curves, which represent the estimated period at which a given loss will be exceeded. When disaggregating the results for each peril, results can be expressed relative to the total exposure in the area considered (Total mean damage ratio, TMDR), or relative to the areas exposed to the different hazards (Relative Mean Damage Ratio, RMDR). Each result provides a different view of the risk, the first, TMDR, shows how each hazard contributes, separately, to the expected losses (Fig. 3a); the second, RMDR, presents how each hazard contributes to loss of its respective exposed buildings (Fig. 3b). In the case study, landslides rank fourth in terms of total exposure and cause the lowest level of losses among all considered hazards. However, this may lead to a misinterpretation of their actual impact, as areas with potential landslide exposure rank second when considering each hazard's relative exposure individually. Further discussion about the results of the MCS approach can be found in Moratalla et al., 2024.

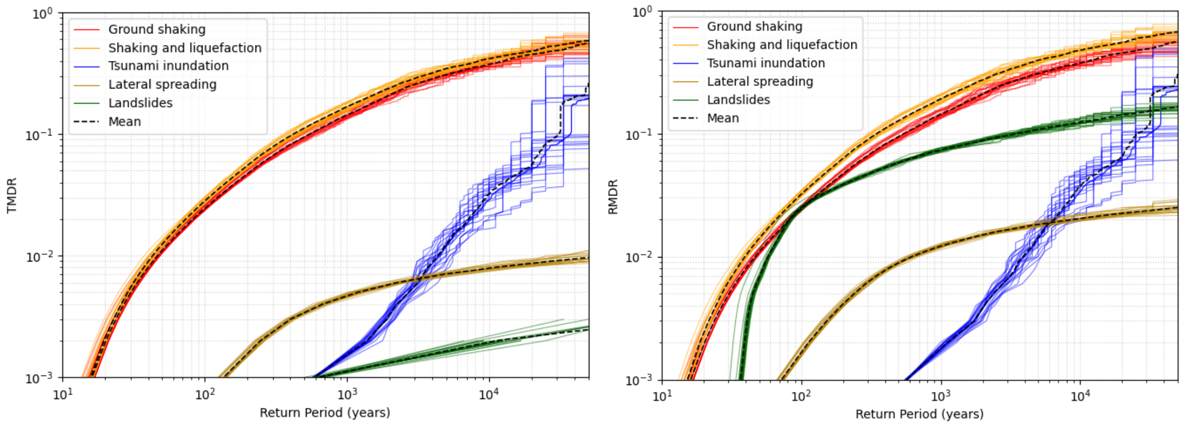

Figure 4: a) Total mean damage ratios (TMDR) and b) Relative mean damage ratios (RMDR) expected in Napier City disaggregated for each peril included in this study (post-earthquake hazards were excluded).

4 CONCLUSION

In this study, we have demonstrated that DEM resolution influences the number of buildings exposed to landslide risk. The higher resolution DEM used, the more realistic the landslide modelling is at capturing impacted areas (both landslide sources and debris inundation). The lower resolution DEM's are more likely to underestimate the number of impacted buildings because topographic features (slope and LSR) are used as a threshold to identify potential landslide source areas, and these features are smoothed in a lower resolution DEM. For the implementation of the Monte Carlo Simulation based framework, to estimate damage from earthquakes and cascading hazard, we used the outputs from the highest resolution landslide hazard models. The framework can generate different types of risk metrics from combined and disaggregated hazards.

5 REFERENCES

Alvioli, M., Marchesini, I., Reichenbach, P., Rossi, M., Ardizzone, F., Fiorucci, F., and Guzzetti, F.: Automatic delineation of geomorphological slope units with r.slopeunits v1.0 and their optimization for landslide susceptibility modeling, *Geosci. Model Dev.*, **9**, 3975–3991, https://doi.org/10.5194/gmd-9-3975-2016, 2016.

Brideau MA, Massey CI, Lukovic B, Morgenstern R. 2020. *Deterministic mapping of potential landslide debris inundation in the Kaikōura District*. Lower Hutt (NZ): GNS Science. 37 p. Consultancy Report 2019/102.

Brideau, M.-A.; de Vilder, S.J.; Massey, C.I.; Mitchell, A.; McDougal, S.; Aaron, J. 2021 *Empirical relationships to estimate the probability of runout exceedance for various landslide types*. p. 321-327; doi: 10.1007/978-3-030-60227-7_36 IN: Guzzetti, F.; Arbanas, S.M.; Reichenbach, P.; Sassa, K.; Bobrowsky, P.T.; Takara, K. Understanding and reducing landslide disaster risk. [WLF 2020]. Volume 2, From mapping to hazard and risk zonation. Cham: Springer. ICL contribution to landslide disaster risk reduction.

Delano, J. E., Howell, A., Clark, K. J., & Stahl, T. A. (2023). Upper plate faults may contribute to the paleoseismic subsidence record along the central Hikurangi subduction zone, Aotearoa New Zealand. Geochemistry, Geophysics, Geosystems, 24(10), e2023GC011060.

GEM. 2019. *The Open Quake-engine user manual, Global Earthquake Model (GEM) Open Quake manual for engine version 3.3.0*. Pavia (IT): GEM Foundation. 189 p. doi:10.13117/GEM.OPENQUAKE.MAN.ENGINE.3.3.0.

Gerstenberger, M., Dissen, R., Rollins, C., Dicaprio, C., Thingbaijim, K., Bora, S., Chamberlain, C., Christophersen, A., Coffey, G., Ellis, S., Iturrieta, P., Johnson, K., Litchfield, N., Nicol, A., Milner, K., Rastin, S., Rhoades, D., Seebeck, H., Shaw, B., Williams, C. (2024). The Seismicity Rate Model for the 2022 Aotearoa New Zealand National Seismic Hazard Model. *Bulletin of the Seismological Society of America*. 114. 10.1785/0120230165.

Jones, K., Massey, C. Townsend, D. Rosser, B. Morgenstern, R., Lukovic, B., Davidson, J., Lyndsell, B., Singeisen, C., Tamsen, D., Carey, J., Villeneuve, M., Mason, D., Wolter, A., Gasston, C., (2024). *Version 3.0 of the landslide inventory for the Mw 7.8 14 November 2016, Kaikōura Earthquake* [Data set]. GNS Science.https://doi.org/10.21420/WX2X-H603.

McDougall, S. (2017). 2014 Canadian Geotechnical Colloquium: Landslide runout analysis—current practice and challenges. *Canadian Geotechnical Journal*, 54(5), 605-620.

McGregor R (1998). *The Hawke's Bay Earthquake: New Zealand's Greatest Natural Disaster*. Art Deco Trust, Napier.

Massey CI, Lukovic B, Huso R, Buxton R, Potter SH. 2021. *Earthquake-induced landslide forecast tool for New Zealand: version 2.0*. Lower Hutt (NZ): GNS Science. 77 p. (GNS Science report; 2018/08). doi:10.21420/G2TP9V.

Massey, C.I.; Lukovic, B. 2023 Earthquake-induced landslide forecast tool for New Zealand: Version 2.1. Lower Hutt, N.Z.: GNS Science. GNS Science report 2023/04.; https://doi.org/10.21420/1ZXA-AB51

Moratalla, J. M., Burbidge, D., Roger, J., Jones, K., Griffin, A., Mueller, C., Uma, S.R., Scheele, F., Bretherton, E. (*Submitted*). Probabilistic Risk Assessment from the Hikurangi Subduction Zone Earthquakes and Cascading Hazards: A Pilot Study in Napier City. 10.2139/ssrn.4854932.

Scheele F.R., Syed Y., Hayes J.L., Paulik R., Inglis S. 2023. Building inventory and vulnerability functions for risk modelling in New Zealand. Lower Hutt (NZ): GNS Science. 42 p. (GNS Science report; 2023/08). doi:10.21420/G34N-V958.

Tonkin & Taylor (2013). "*Liquefaction vulnerability study*". Report for the Earthquake Commission, Wellington, New Zealand, 50 pp. https://www.eqc.govt.nz/sites/public_files/documents/liquefaction-vulnerability-study-final.pdf

Williams, C. A., Eberhart-Phillips, D., Bannister, S., Barker, D. H. N., Henrys, S., Reyners, M., & Sutherland, R. (2013). Revised interface geometry for the Hikurangi subduction zone, New Zealand. *Seismological Research Letters*, 84(6), 1066–1073. DOI: 10.1785/0220130035

Zhang G, Robertson PK and Brachman RWI (2004). "Estimating liquefaction-induced lateral displacements using the standard penetration test or cone penetration test". *ASCE Journal of Geotechnical and Geoenvironmental Engineering*, 130: 861–871.

6 ACKNOWLEDGMENTS

This project was supported by the New Zealand Ministry of Business, Innovation and Employment (MBIE) through the Hazards and Risk Mitigation Programme (SSIF contract C05X1702).

The authors would also like to thank Biljana Lukovic and Saskia de Vilder for expert guidance about the landslide hazard and risk analysis.